Electronic Supplementary Material (ESI) for Analyst.

Supplementary Information

A novel dehydroabietic acid-based fluorescent probe with three channels for detection of Cu^{2+}/Zn^{2+}/ClO^{-}†

Lu Sun, Zhonglong Wang, Linlin Chen, Xuebao Sun, Zihui Yang, Wen Gu*

Jiangsu Provincial Key Lab for the Chemistry and Utilization of Agro-forest Biomass, Jiangsu Key Lab of Biomass-based Green Fuels and Chemicals, Jiangsu Co-Innovation Center of Efficient Processing and Utilization of Forest Resources, College of Chemical Engineering, Nanjing Forestry University, Nanjing 210037, P. R. China. E-mail address: njguwen@163.com;

† Electronic supplementary information (ESI) available. See DOI:

Experimental procedures

Instruments and materials

Melting points were determined by an OptiMelt automated melting point system (Stanford Research System, USA) and were uncorrected. Fluorescence and UV-vis spectral data were recorded by an LS55 fluorescence spectrophotometer (Perkin Elmer, USA) and a UV-2450 spectrophotometer (Shimadzu, Japan). FT-IR spectra were recorded by a Nicolet Summit FTIR Spectrometer (Thermo Fisher, USA). HR-MS spectra were collected by a Waters G2-xs (LC/ESI) instrument (Waters, USA). ^{1}H NMR and ^{13}C NMR were obtained by a Bruker AVANCEIIIHD 600 MHz spectrometer (Bruker, Germany) with TMS as the internal standard. The fluorescence imagings in cells and zebrafishes were carried out by a Zeiss LSM 570 laser confocal microscope (Carl Zeiss, Germany). Cytotoxicity of cells was tested by microplate reader (Thermo Fischer Scientifics, USA). All reagents and solvents were analytical grade from Shanghai Chemical Reagent Company (Shanghai, China) and Energy Chemical (Shanghai, China) without further treatment.

Cytotoxicity test

MCF-7 cells were cultured in DMEM medium with 10% fetal bovine serum (PBS), 1% penicillin, and streptomycin at 37°C with 5% CO_2 and seeded in 96-well microplates. After 24 h, the cells were treated by **CPS** with different concentrations (0, 10, 20, 30 and 40 μM) for two days. Subsequently, MTT solution (5 mg/mL, 10 μL) was injected into each well and the cells were incubated for additional 4 h. MTT solution was then removed and the cells were washed by PBS buffer. At last, the formed blue formazan crystals were dissolved in DMSO (150 μL) and the absorbance can be obtained by a microplate reader (Thermo Fischer Scientifics, USA) to test the level of toxicity.

Bioimaging

MCF-7 cells were cultured in DMEM medium with 10% fetal bovine serum (FBS),

1% penicillin, and streptomycin at 37°C with 5% CO_2 for 24 hours. Then the cells were treated by the probe **CPS** (10 μM) in the 6-well flat-bottomed plates. After 3 h of incubation, the excess probes were removed and the wells were washed with PBS buffer. Subsequently, these cells were treated with different concentrations of ClO^-, Cu^{2+} or Zn^{2+} (15 μM, 30 μM) for 30 minutes. Finally, the cells were washed with PBS for three times and imaged under the Laser confocal microscope (Carl Zeiss, Germany).

Zebrafish eggs were bought from Shanghai FishBio Co., Ltd. and cultured with a nutrient solution in a thermostat water bath at 26°C. After 5 days, the juvenile zebrafishes were put in 6-well flat-bottomed plates with deionized water (1×10^4/well). Part of the zebrafishes was exposed to **CPS** (10 μM, 25 min) as the control group. The other fishes treated with **CPS** (10 μM, 25 min) were further treated with ClO^-, Cu^{2+} or Zn^{2+} (5 μM, 30 μM) for 30 min. Subsequently, the samples were washed three times with water and anesthetized on glass slides with MS-22. Finally, the fishes were imaged under the Laser confocal microscope (Carl Zeiss, Germany).

Supplementary Tables and Figures

Table. S1. Previously reported fluorescent probes sensing ClO^-, Cu^{2+} and Zn^{2+}.

Fig. S1. ^1H NMR spectra of probe **CPS** (600 MHz, DMSO-d_6).

Fig. S2. ^{13}C NMR spectra of probe **CPS** (151 MHz, DMSO-d_6)

Fig. S3. HR-MS of probe **CPS**.

Fig. S4. (a) Interference of the **CPS** + Cu^{2+} sensor over the various cations in EtOH/H_2O (v/ v =2/8, pH =7.1) in the presence of various other ions (20 μM). (b) The intensity ratio (F_{440nm}/F_{515nm}) of **CPS** (10 μM) and Zn^{2+} (20 μM) in EtOH/H_2O (v/ v =2/8, pH =7.1) in the presence of various other ions (20 μM). (c) The intensity ratio (F_{467nm}/F_{515nm}) of **CPS** (10 μM) and ClO^- (20 μM) in EtOH/H_2O (v/v = 2/8, pH =7.1) in the presence of various other ions (20 μM)

Fig.S5. (a) Time-dependent fluorescent intensity of probe **CPS** (10 μM) in the absence and presence of Cu^{2+} (20 μM). (b) Time-dependent fluorescent intensity ratio (F_{440nm}/F_{515nm}) of probe **CPS** (10 μM) in the absence and presence of Zn^{2+} (20 μM). (c) Time-dependent fluorescent intensity ratio (F_{467nm}/F_{515nm}) of probe **CPS** (10 μM) in

the absence and presence of ClO^- (20 μM).

Fig.S6. (a) Fluorescent intensity of probe **CPS** (10 μM) in the absence and presence of Cu^{2+} (20 μM) within 200 min. (b) Fluorescent intensity ratio (F_{440nm}/F_{515nm}) of probe **CPS** (10 μM) in the absence and presence of Zn^{2+} (20 μM) within 200 min. (c) Fluorescent intensity ratio (F_{467nm}/F_{515nm}) of probe **CPS** (10 μM) in the absence and presence of ClO^- (20 μM) within 200 min.

Fig.S7. (a) Fluorescence intensity changes of **CPS** (10 μM) and **CPS**-Cu^{2+} at different pH. (b) Fluorescence intensity ratio (F_{440nm}/F_{515nm}) changes of **CPS** (10 μM) and **CPS**-Zn^{2+} at different pH. (c) Fluorescence intensity ratio (F_{467nm}/F_{515nm}) changes of **CPS** (10 μM) and **CPS**-ClO^- at different pH.

Fig. S8. (a) Job's plots of **CPS**-ClO^- complexes in ethanol solution. (b) Job's plots of **CPS**-Cu^{2+} complexes in ethanol solution. (c) Job's plots of **CPS**-Zn^{2+} complexes in ethanol solution.

Fig. S9. ^1H NMR spectra of **CPS** upon the addition of different equivalents of ClO^-, Cu^{2+} and Zn^{2+}.

Fig.S10. FT-IR spectra of **CPS**, **CPS**-Zn^{2+}, **CPS**-Cu^{2+}, and **CPS**-ClO^- complexes

Fig.S11. ESI-MS spectra of **CPS**-Cu^{2+} complex

Fig.S12. ESI-MS spectra of **CPS**-Zn^{2+} complex

Fig.S13. ESI-MS spectra of **CPS**-ClO^- complex.

Fig. S14. (a) Fluorescence intensity ratio (F_{467nm}/F_{515nm}) changes of **CPS** upon alternate addition of ClO^- and EDTA. (b) Fluorescence intensity ratio (F_{440nm}/F_{515nm}) changes of **CPS** upon alternate addition of Zn^{2+} and EDTA. (c) Fluorescence intensity changes of **CPS** upon alternate addition of Cu^{2+} and EDTA.

Fig. S15. Optimized molecular configurations and frontier molecular orbital profiles of probe **CPS** and complex **CPS**+ClO^-, **CPS**+Cu^{2+} and **CPS**+Zn^{2+}.

Fig.S16. Cell viability of MCF-7 cells incubated with different concentrations of **CPS**

Fig.S17. Fluorescent bleaching experiment of zebrafish from 10 min to 60 min Scale.

Table. S1. Previously reported fluorescent probes sensing ClO^-, Cu^{2+} and Zn^{2+}.

Probe	Response mode	Response time	LOD	pH range	Detection diversity	Ref
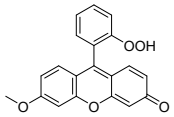	Turn on	1 min	55 nM	7~10	Cu^{2+}	[1]
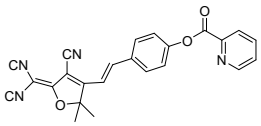	Turn on	10 min	54 nM	6~9	Cu^{2+}	[2]
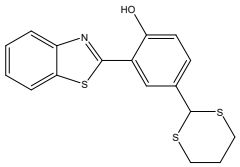	Cu^{2+}: Turn off Hg^{2+}: Ratiometric	35min 8min	2.4 nM 7.6 nM	5-10 5-9	Cu^{2+} Hg^{2+}	[3]
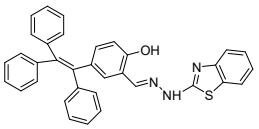	Turn on	20 min	21 nM	4~12	Zn^{2+}	[4]
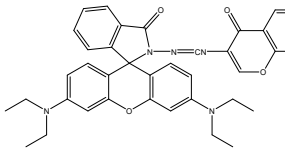	Ratiometric	6 min	0.335 μM	No data	Zn^{2+}	[5]
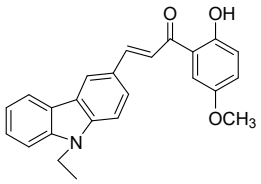	Turn on	10 min	0.3 μM	6~9	ClO^-	[6]
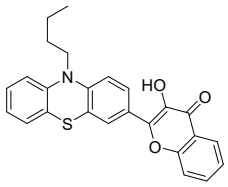	Ratiometric	10 min	6.6 nM	6~10	ClO^-	[7]
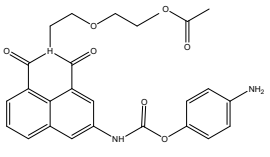	Ratiometric	within 20s	0.7 μM	6~11	ClO^-	[8]
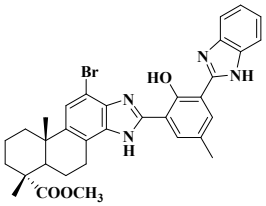	(Cu^{2+}) Turn off (Zn^{2+}) Ratiometric (ClO^-) Ratiometric	20 s 20 s 15 s	3.8 nM 0.253 μM 0.452 μM	2~10	Cu^{2+} Zn^{2+} ClO^-	**This work**

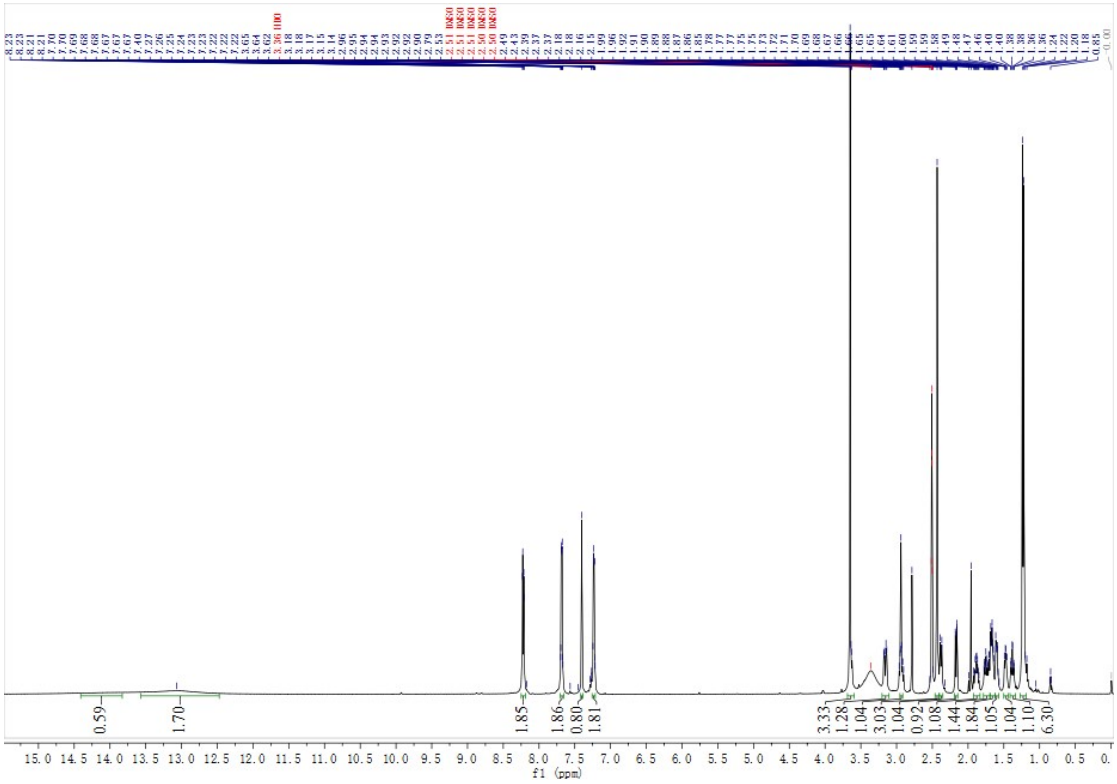

Fig. S1. ^{1}H NMR spectra of probe **CPS** (600 MHz, DMSO-d_6).

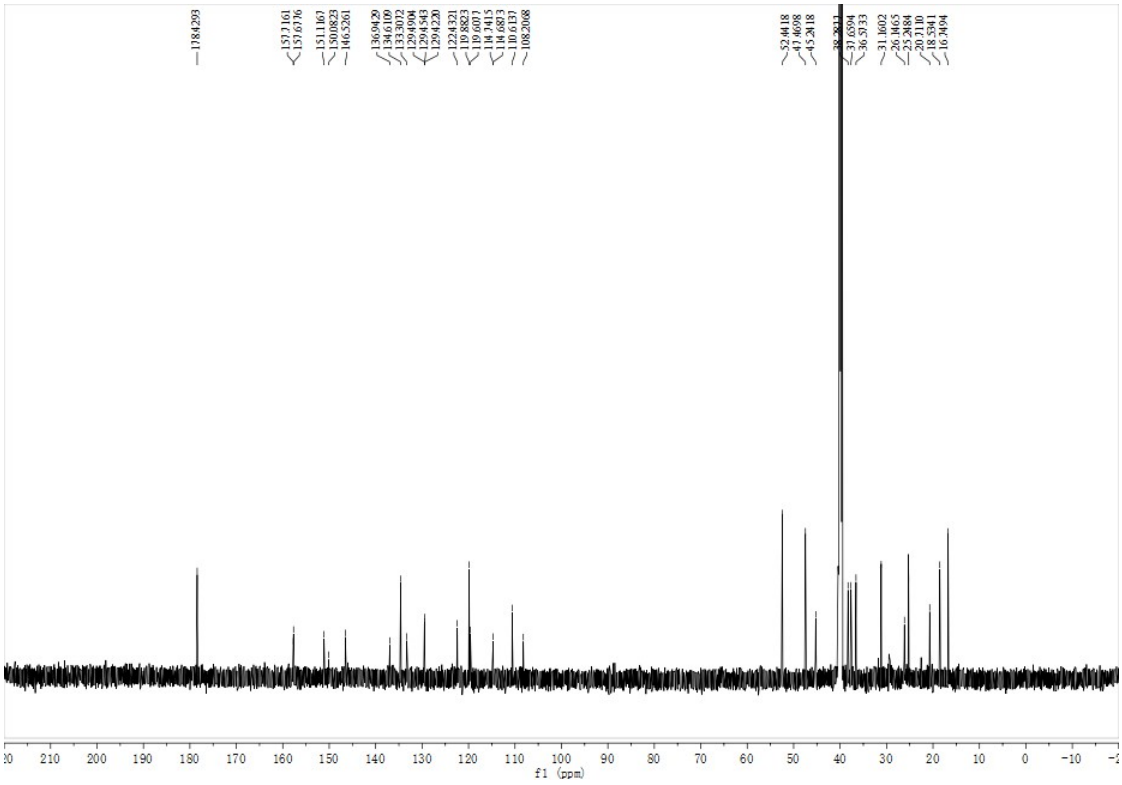

Fig. S2. ^{13}C NMR spectra of probe **CPS** (151 MHz, DMSO-d_6).

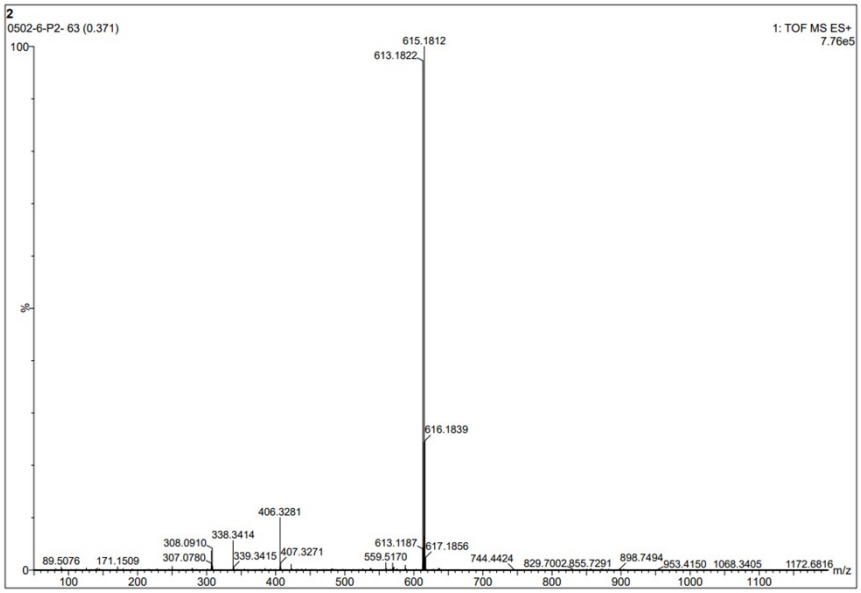

Fig. S3. HR-MS of probe **CPS.**

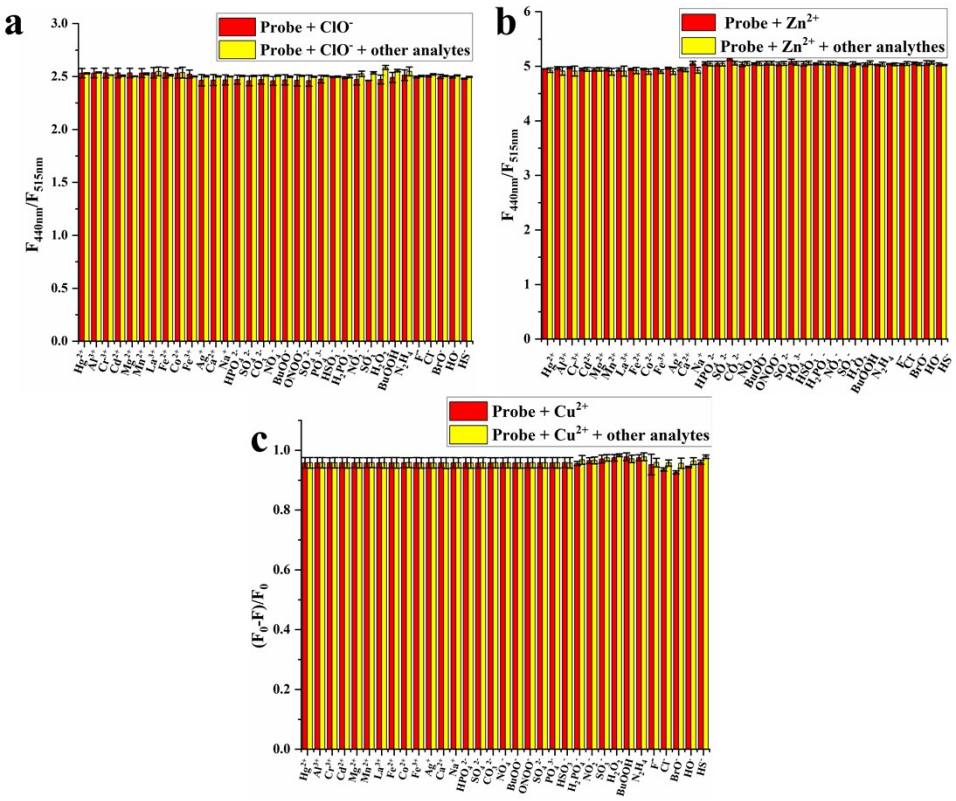

Fig. S4. (a) Interference of the **CPS** + Cu^{2+} sensor over the various cations in EtOH/H_2O (v/v = 2/8, pH = 7.1) in the presence of various other ions (20 μM). (b) The intensity ratio (F_{440nm}/F_{515nm}) of **CPS** (10 μM) and Zn^{2+} (20 μM) in EtOH/H_2O (v/v = 2/8, pH = 7.1) in the presence of various other ions (20 μM). (c) The intensity ratio (F_{467nm}/F_{515nm}) of **CPS** (10 μM) and ClO^- (20 μM) in EtOH/H_2O (v/v = 2/8, pH = 7.1) in the presence of various other ions (20 μM).

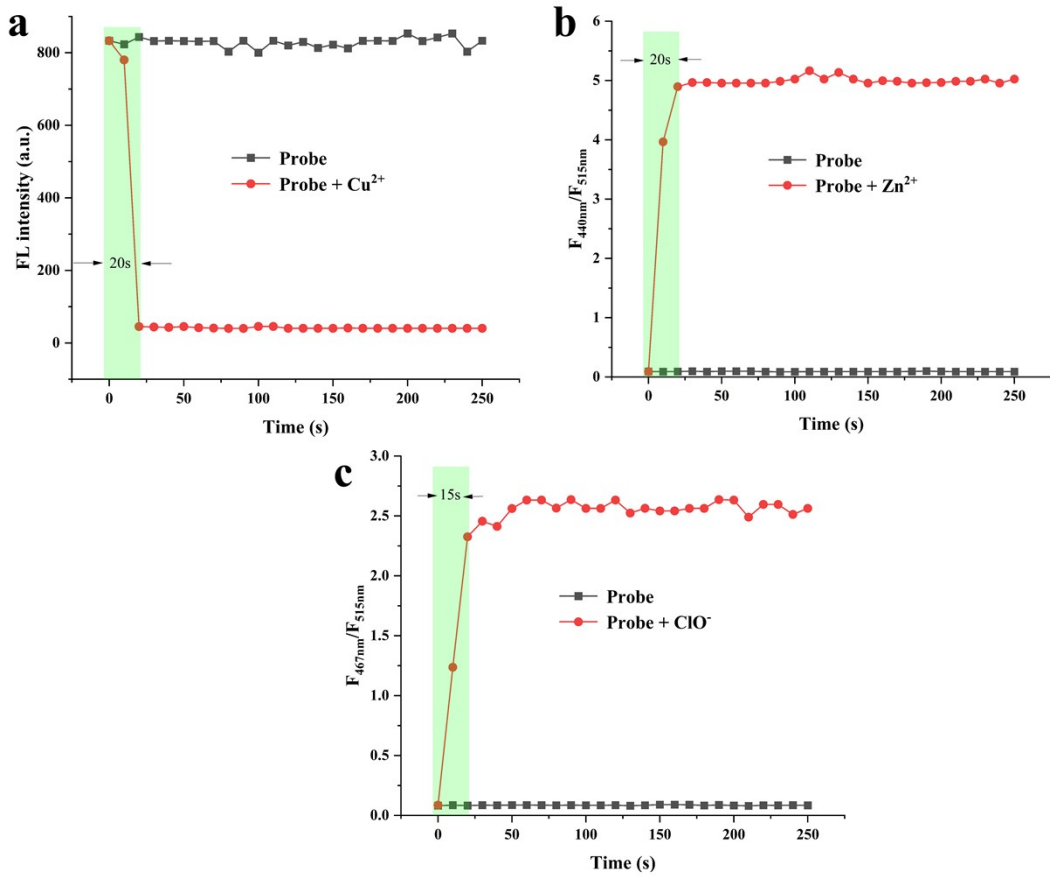

Fig. S5. (a) Time-dependent fluorescent intensity of probe **CPS** (10 μM) in the absence and presence of Cu^{2+} (20 μM). (b) Time-dependent fluorescent intensity ratio (F_{440nm}/F_{515nm}) of probe **CPS** (10 μM) in the absence and presence of Zn^{2+} (20 μM). (c) Time-dependent fluorescent intensity ratio (F_{467nm}/F_{515nm}) of probe **CPS** (10 μM) in the absence and presence of ClO^- (20 μM).

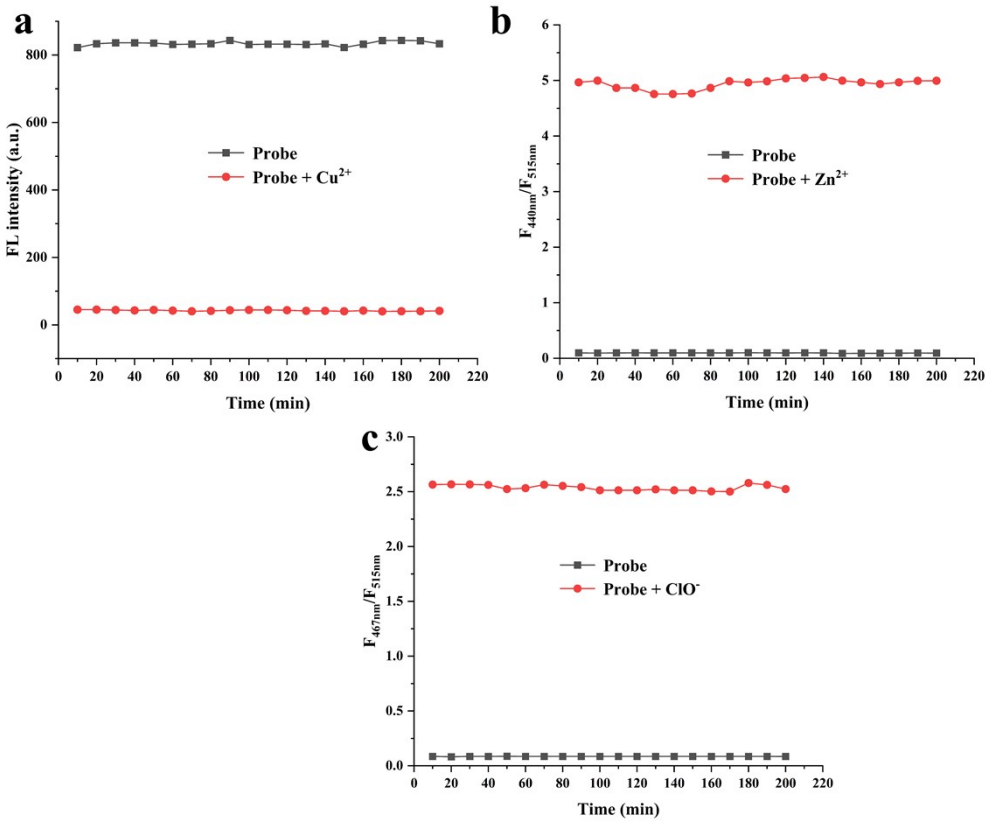

Fig. S6. (a) Fluorescent intensity of **CPS** (10 μM) in the absence and presence of Cu^{2+} (20 μM) within 200 min. (b) Fluorescent intensity ratio (F_{440nm}/F_{515nm}) of **CPS** (10 μM) in the absence and presence of Zn^{2+} (20 μM) within 200 min. (c) Fluorescent intensity ratio (F_{467nm}/F_{515nm}) of **CPS** (10 μM) in the absence and presence of ClO^- (20 μM) within 200 min.

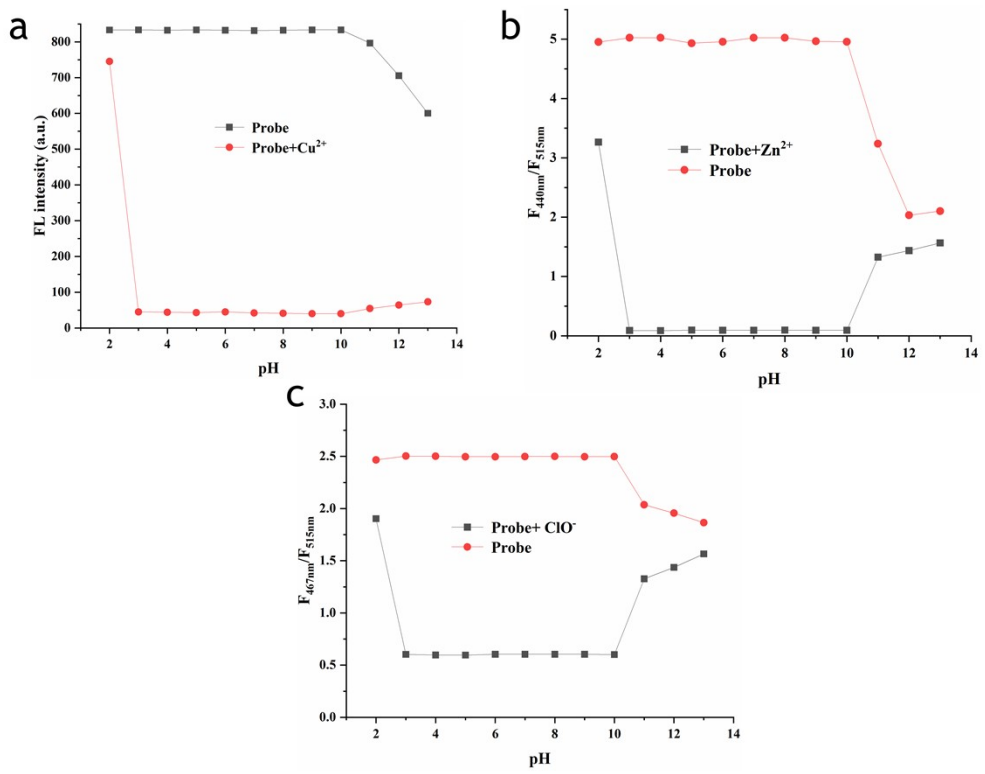

Fig. S7. (a) Effects of pH on fluorescence intensity of **CPS** (10 μM) before and after adding Cu^{2+} (20 μM) in EtOH/H_2O (v/v = 2/8, pH = 7.1). (b) Effects of pH on fluorescence intensity ratio ($F_{440\ nm}/F_{515\ nm}$) of **CPS** (10 μM) before and after adding Zn^{2+} (20 μM) in EtOH/H_2O (v/v = 2/8, pH = 7.1). (c) Effects of pH on fluorescence intensity ratio ($F_{467\ nm}/F_{515\ nm}$) of **CPS** (10 μM) before and after adding ClO^- (20 μM) in EtOH/H_2O (v/v = 2/8, pH = 7.1).

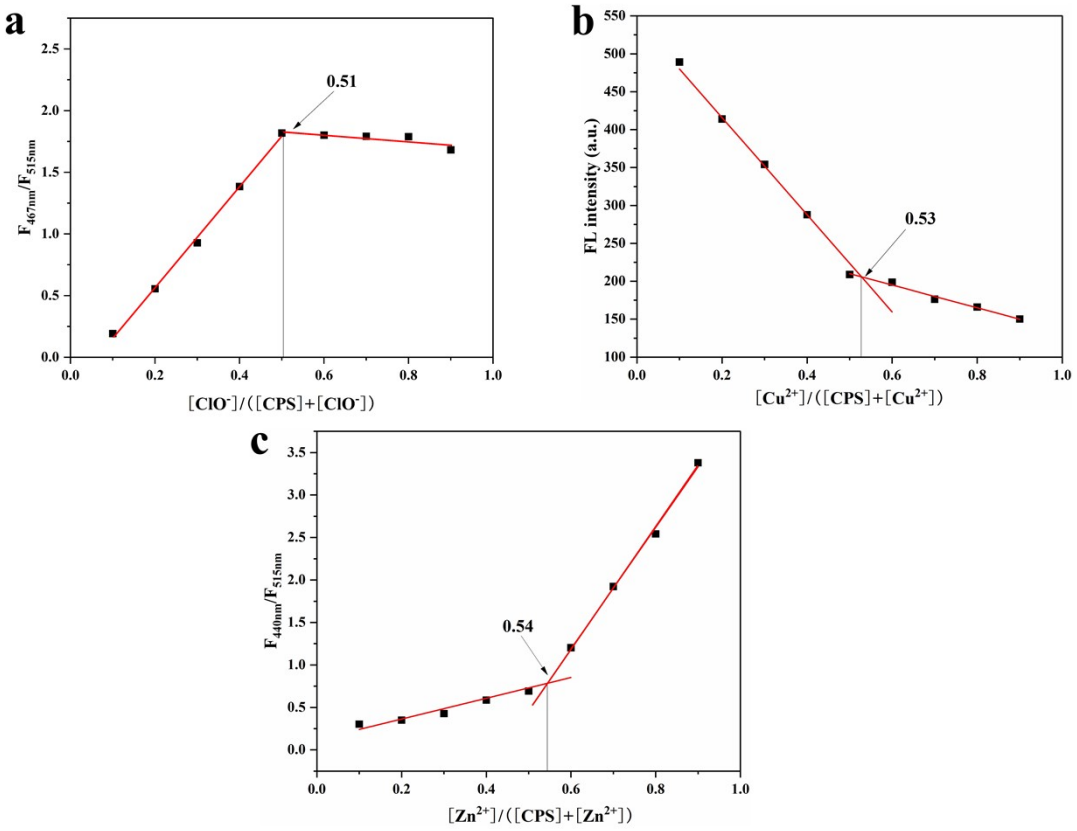

Fig. S8. (a) Job's plots of **CPS**-ClO^- complexes in ethanol solution. (b) Job's plots of **CPS**-Cu^{2+} complexes in ethanol solution. (c) Job's plots of **CPS**-Zn^{2+} complexes in ethanol solution.

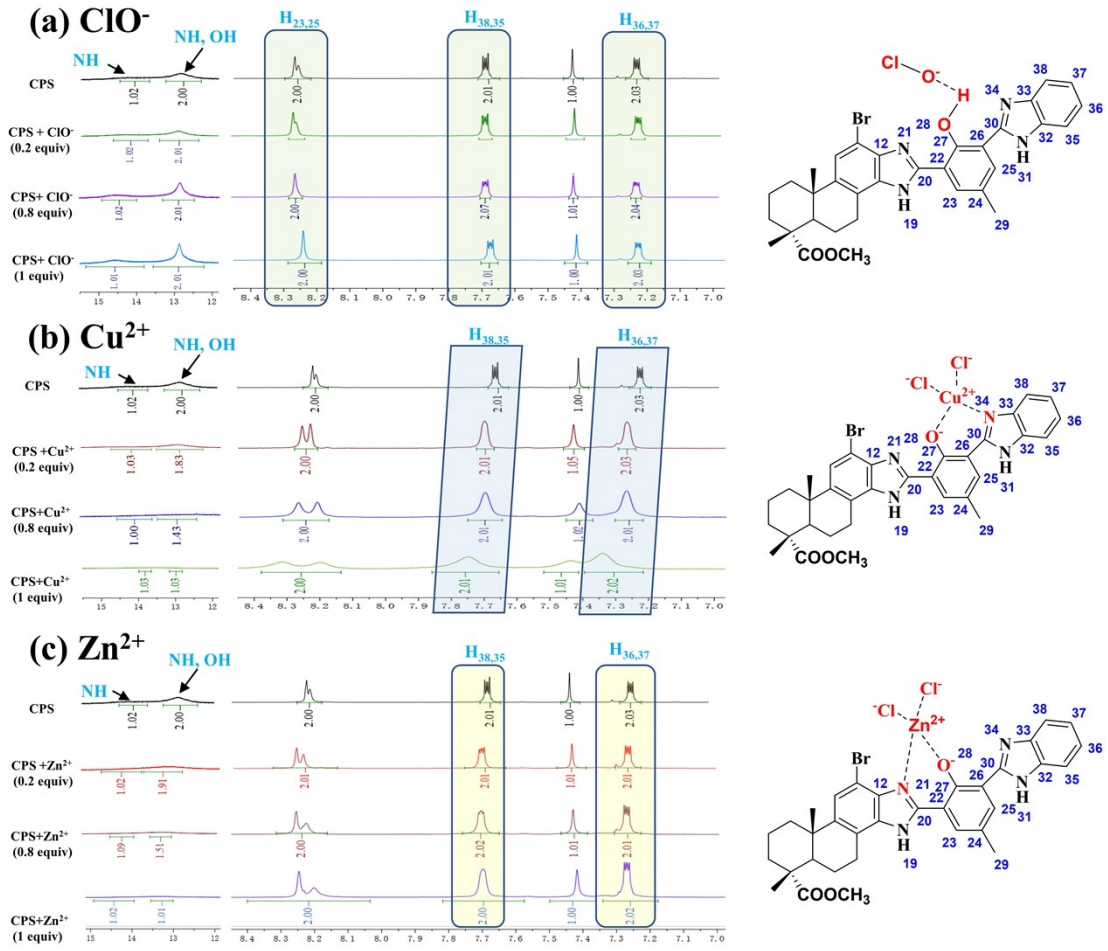

Fig. S9. ^{1}H NMR spectra of **CPS** upon the addition of different equivalents of ClO^{-}, Cu^{2+} and Zn^{2+}.

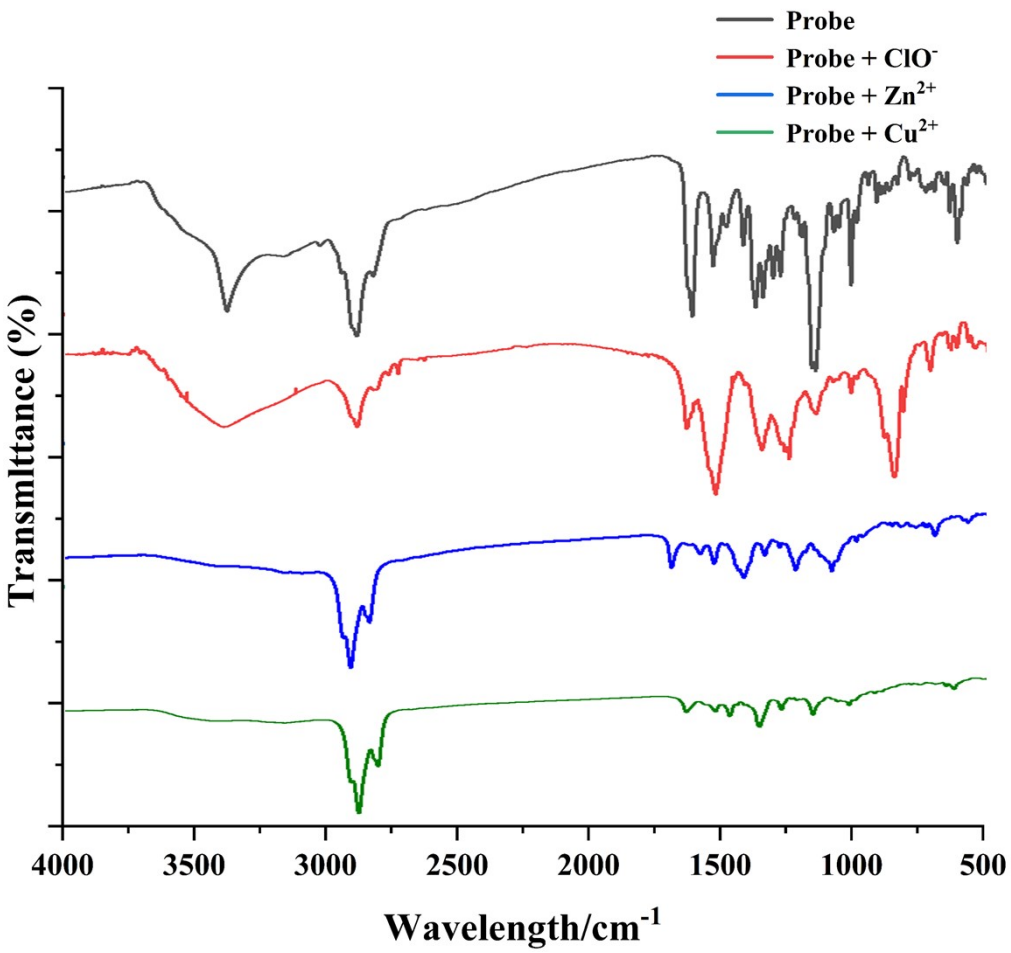

Fig. S10. FT-IR spectra of **CPS**, **CPS**-ClO^{-}, **CPS**-Zn^{2+} and **CPS**-Cu^{2+} complexes.

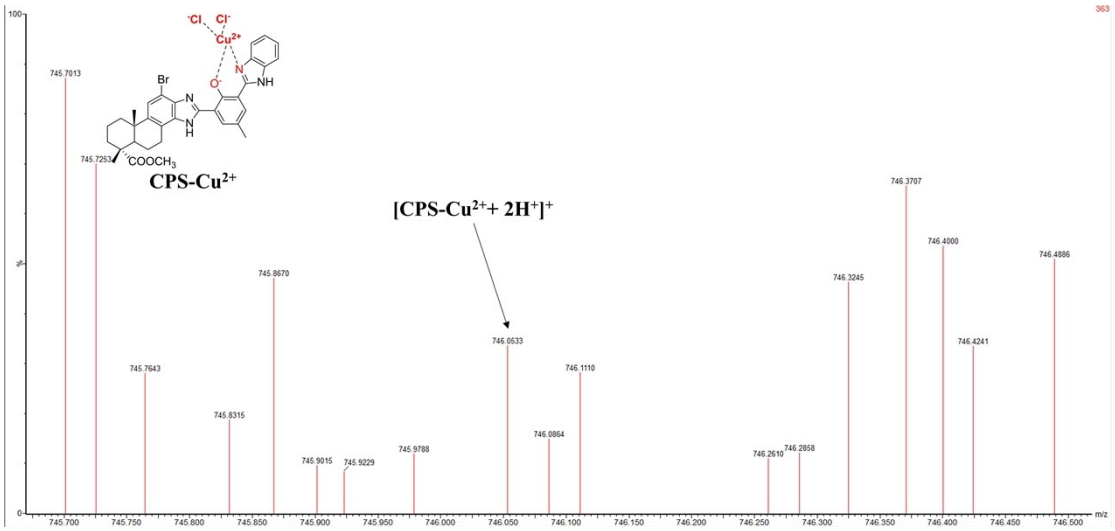

Fig. S11. ESI-MS spectra of **CPS**-Cu^{2+} complex.

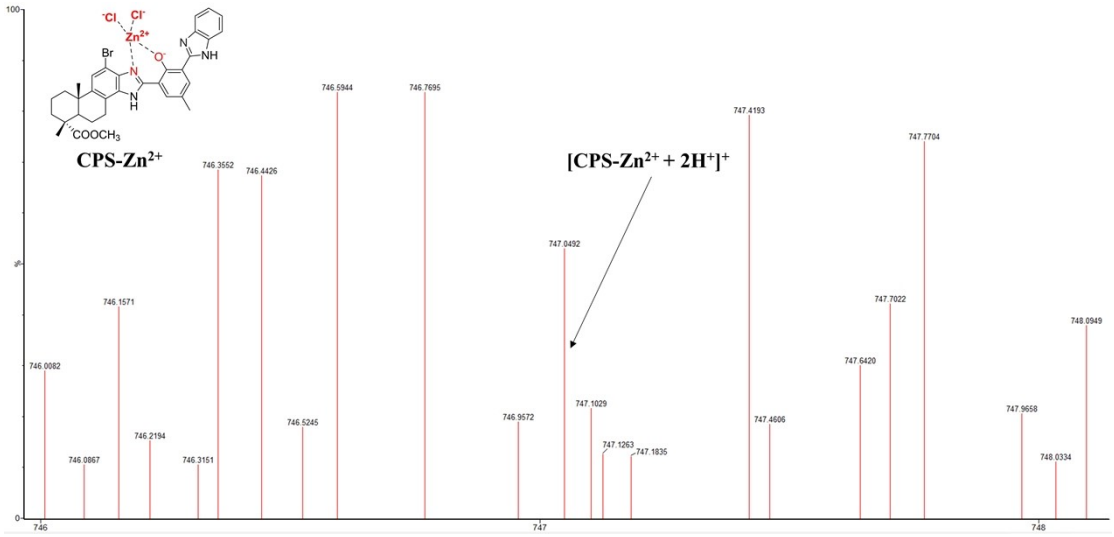

Fig. S12. ESI-MS spectra of **CPS**-Zn^{2+} complex.

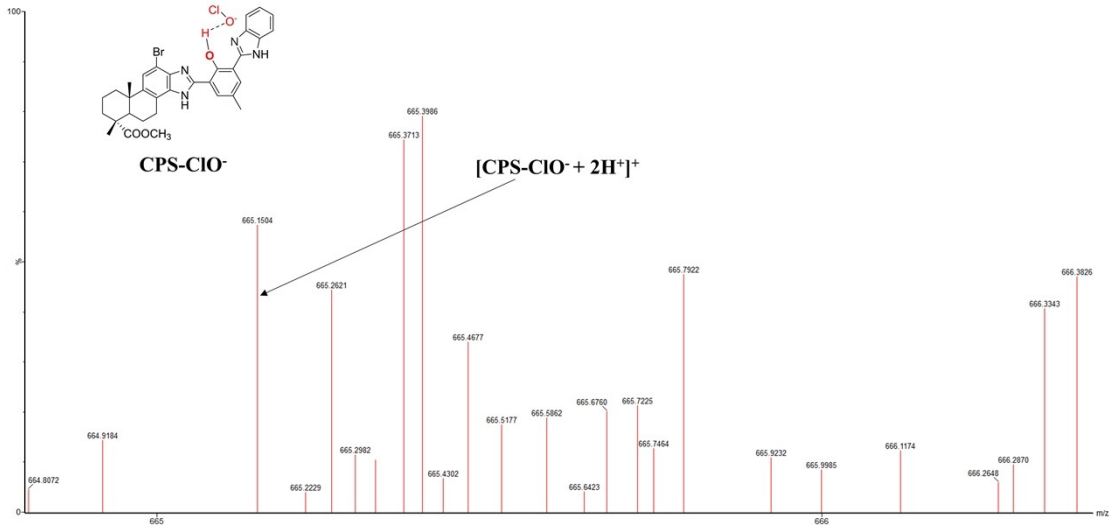

Fig. S13. ESI-MS spectra of **CPS**-ClO^{-} complex.

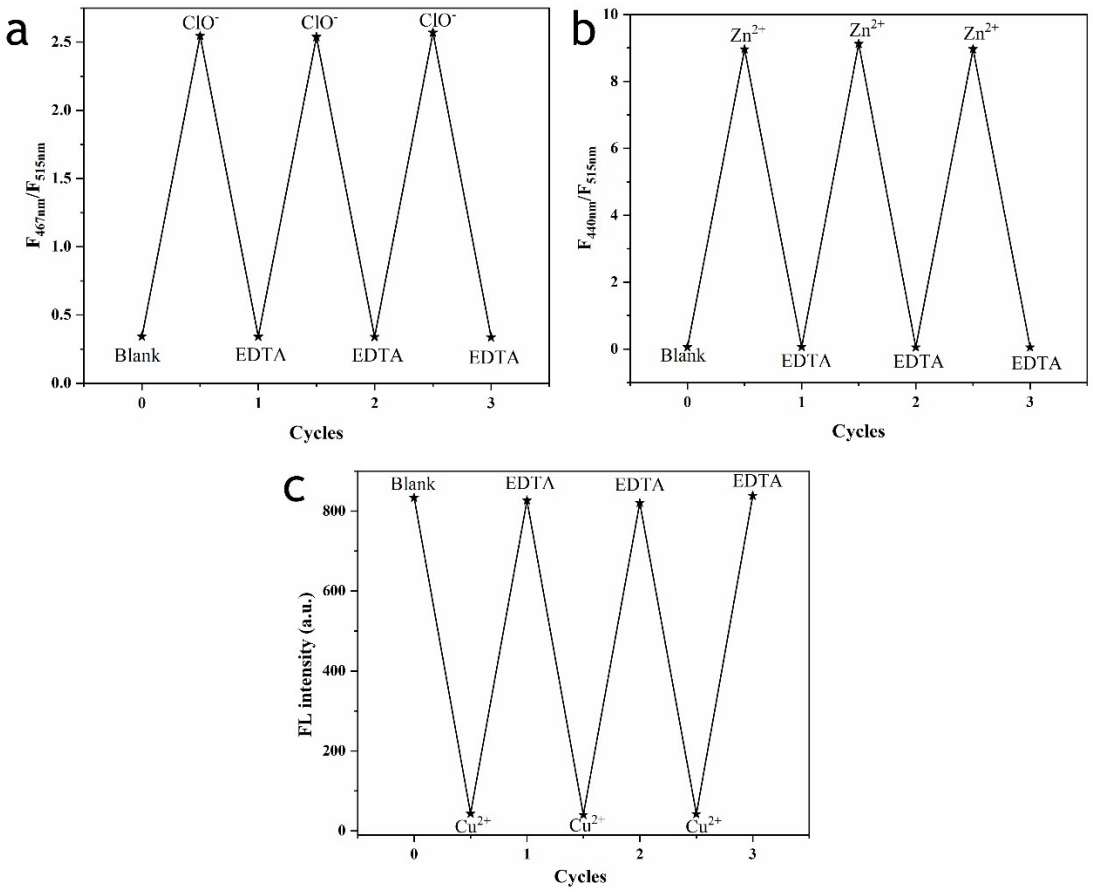

Fig. S14. (a) Fluorescence intensity ratio (F_{467nm}/F_{515nm}) of **CPS** upon alternate addition of ClO^- and EDTA. (b) Fluorescence intensity ratio (F_{440nm}/F_{515nm}) of **CPS** upon alternate addition of Zn^{2+} and EDTA. (c) Fluorescence intensity of **CPS** upon alternate addition of Cu^{2+} and EDTA.

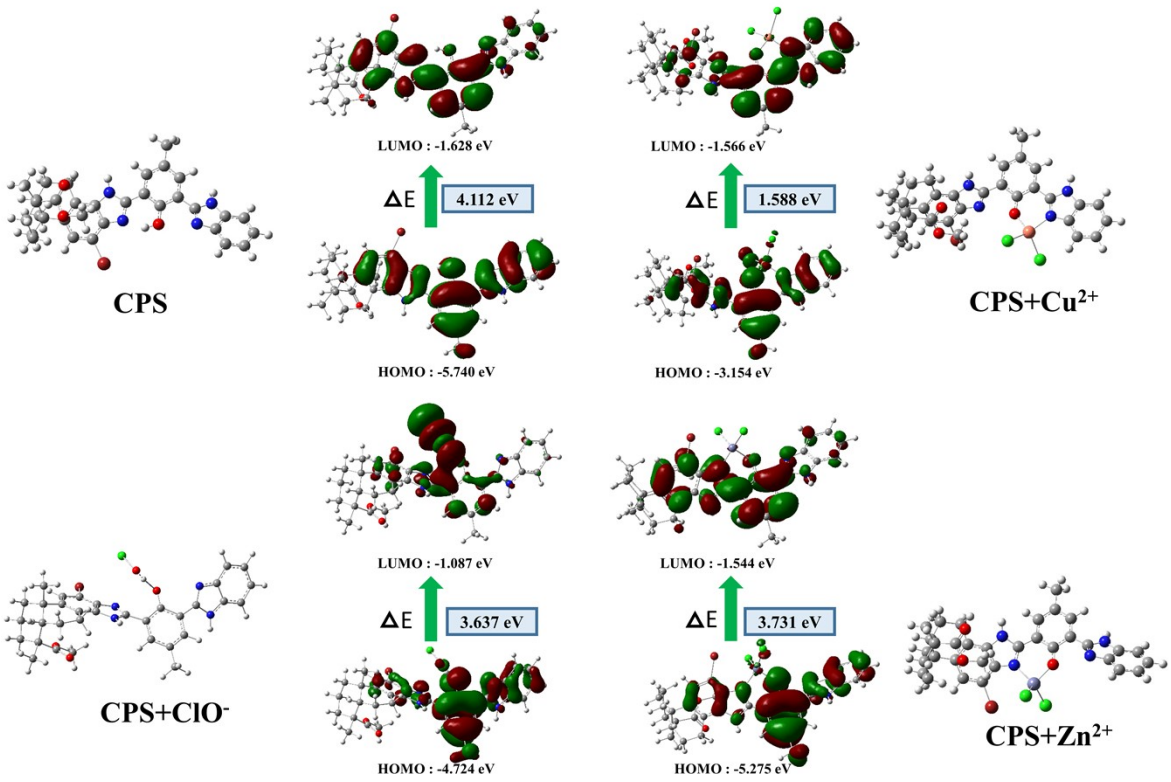

Fig. S15. Optimized molecular configurations and frontier molecular orbital profiles of probe **CPS** and complex **CPS**+ClO^-, **CPS**+Cu^{2+} and **CPS**+Zn^{2+}.

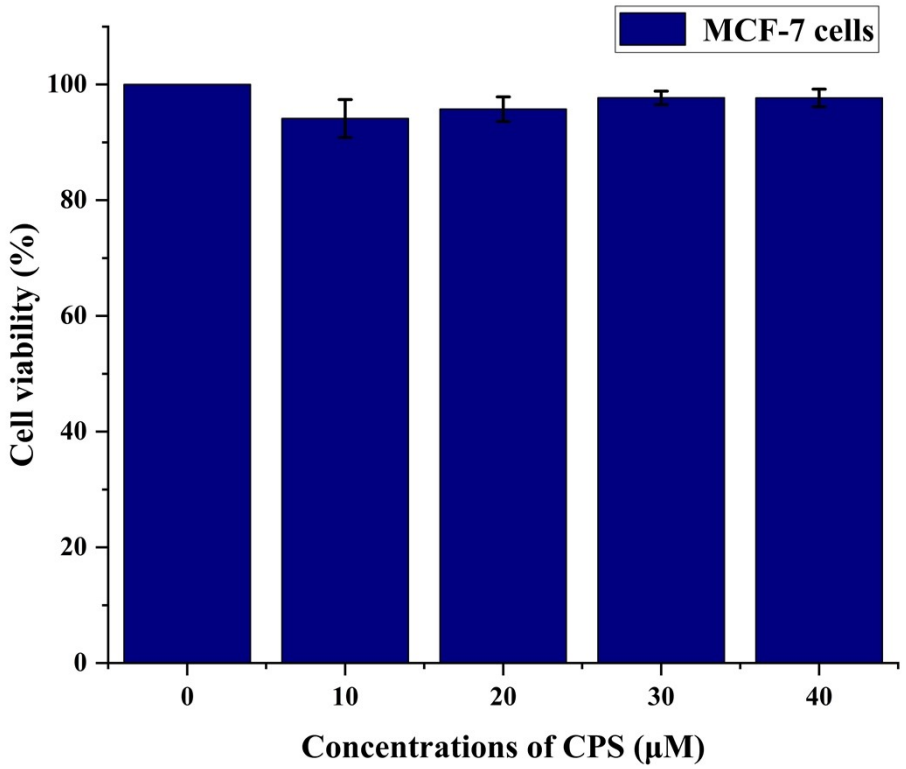

Fig. S16. Cell viability of MCF-7 cells incubated with different concentrations of **CPS.**

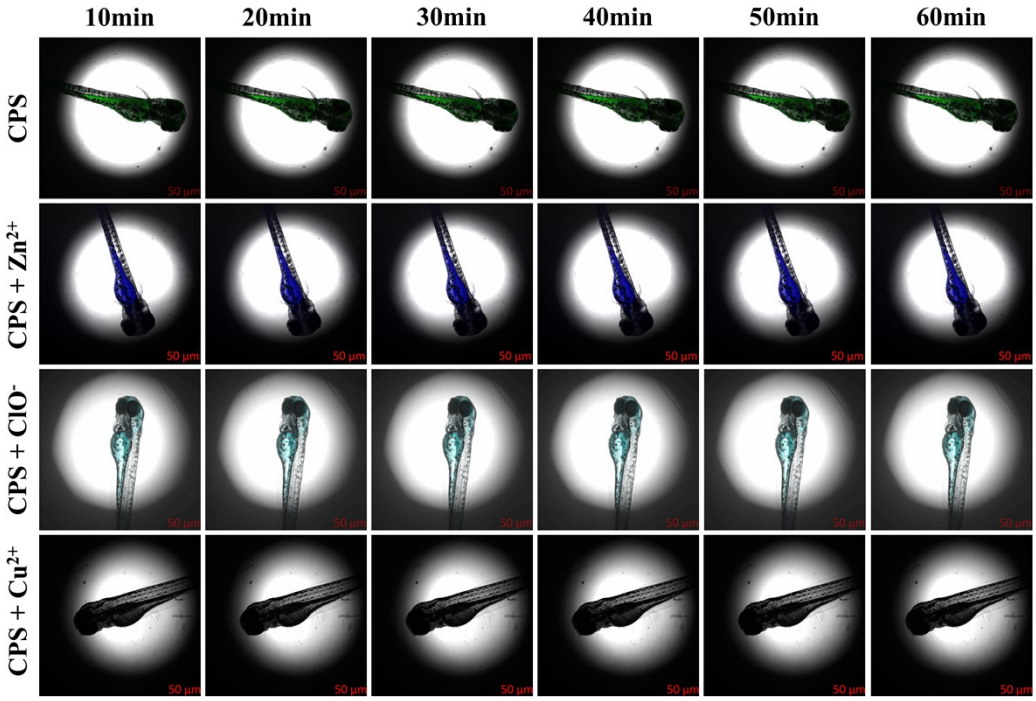

Fig. S17. Fluorescent bleaching experiment of zebrafish from 10 min to 60 min Scale.

References

1 D. Zhu, Y. Luo, X. Yan, W. Xie, W. Cai, X. Zhong, *RSC Adc.*, 2016, **6,** 87110-87114.

2 K. H. Nguyen, Y. Hao, K. Zeng, X. Wei, S. Yuan, F. Li, S. G. Fan, M. T. Xu and Y. N. Liu, *J. Photochem. Photobiol. A*, 2018, **358,** 201-206.

3 B. Gu, L. Huang, W. Su, X. Duan, H. Li and S. Yao, *Anal. Chim. Acta*, 2017, **954,** 97-104.

4 J. Wang, L. Lu, C. Wang, M. Wang, J. Ju, J. Zhu and T. Sun, *New J. Chem.*, 2020, **44,** 15426-15431.

5 L. M. Liu and Z. Y. Yang, *J. Photochem. Photobiol. A*, 2018, **364,** 558-563.

6 J. Chao, Y. Duan, Y. Zhang, F. Huo, C. Yin, M. Xu and M. Li, *Chem. Pap.*, 2019, **74,** 1171-1176.

7 L. He, Y. Zhang, H. Q. Xiong, J. P. Wang, Y. N. Geng, B. H. Wang, Y. G. Wang, Z. G. Yang and X. Z. Song, *Dyes Pigm.*, 2019, **166,** 390-394.

8 T. Guo, L. Cui, J. N. Shen, R. Wang, W. P. Zhu, Y. F. Xu, X. H. Qian, *Chem. Commun.*, 2013, **49,** 1862-1864.